View metadata, citation and similar papers at core.ac.uk

brought to you by CORE

provided by Missouri University of Science and Technology (Missouri S&T): Scholars' Mine

Missouri University of Science and Technology

Scholars' Mine

Chemistry Faculty Research & Creative Works

Chemistry

01 May 2007

Structural, Magnetic, and Transport Properties of Zr-substituted $La_{0.7}Sr_{0.3}MnO_3$

Minseob Kim

Jinbo Yang

Qingsheng Cai

William Joseph James
Missouri University of Science and Technology, wjames@mst.edu

et. al. For a complete list of authors, see https://scholarsmine.mst.edu/chem_facwork/2660

Follow this and additional works at: https://scholarsmine.mst.edu/chem_facwork

 Part of the Chemistry Commons, and the Physics Commons

Recommended Citation

M. Kim et al., "Structural, Magnetic, and Transport Properties of Zr-substituted $La_{0.7}Sr_{0.3}MnO_3$," *Journal of Applied Physics*, vol. 102, no. 1, pp. 013531-1-013531-8, American Institute of Physics (AIP), May 2007. The definitive version is available at https://doi.org/10.1063/1.2749472

This Article - Journal is brought to you for free and open access by Scholars' Mine. It has been accepted for inclusion in Chemistry Faculty Research & Creative Works by an authorized administrator of Scholars' Mine. This work is protected by U. S. Copyright Law. Unauthorized use including reproduction for redistribution requires the permission of the copyright holder. For more information, please contact scholarsmine@mst.edu.

Structural, magnetic, and transport properties of Zr-substituted $La_{0.7}Sr_{0.3}MnO_3$

M. S. Kim and J. B. Yang[a)]
Materials Research Center, University of Missouri—Rolla, Rolla, Missouri 65409
and Department of Physics, University of Missouri—Rolla, Rolla, Missouri 65409

Q. Cai
Department of Physics, University of Missouri—Columbia, Columbia, Missouri 65211

W. J. James and W. B. Yelon
Materials Research Center, University of Missouri—Rolla, Rolla, Missouri 65409
and Department of Chemistry, University of Missouri—Rolla, Rolla, Missouri 65409

P. E. Parris
Department of Physics, University of Missouri—Rolla, Rolla, Missouri 65409

S. K. Malik
Tata Institute of Fundamental Research, Colaba, Mumbai 400-005, India

(Received 7 March 2007; accepted 9 May 2007; published online 13 July 2007)

Zr-substituted perovskites $La_{0.7}Sr_{0.3}Mn_{1-x}Zr_xO_3$ with $0 \leqslant x \leqslant 0.20$ were investigated by neutron diffraction (ND), magnetization, electric resistivity, and magnetoresistance measurements. ND refinements reveal that substituted Zr^{4+} goes only to the Mn site. Because of its large size, this leads to a Zr-solubility limit at $x \leqslant 0.10$. The $x \leqslant 0.10$ samples exhibit a rhombohedral structure (space group $R\bar{3}c$) from 10 K to room temperature. For the $x \leqslant 0.10$ samples, the cell parameters a and c, and volume increase continuously with increasing Zr content. In addition, the structural distortion of the MnO_6 octahedra increases with increasing Zr content. Zr-substituted $La_{0.7}Sr_{0.3}MnO_3$ exhibits metallic behavior at low temperature. The field dependent resistivity suggests that electron-electron scattering is dominant and a two-magnon scattering process emerges with increasing temperature. The contribution from the two-magnon scattering in resistivity becomes larger with increasing Zr content. A maximum magnetoresistance (MR_{max}) of 35% is obtained for the $x=0.03$ sample at $H=5$ T. The MR_{max} shifts to a higher temperature region upon application of an external magnetic field. © *2007 American Institute of Physics*. [DOI: 10.1063/1.2749472]

I. INTRODUCTION

The magnetotransport properties of the substituted manganese perovskites, $La_{1-x}D_xMnO_3$ (D=Sr,Ca,Pb,Ba), have been a subject of great interest because of anomalous magnetic and transport properties such as colossal magnetoresistance (CMR), metal to insulator transitions (MITs), and lattice dynamics associated with the phase transitions.[1–5]

The large magnetoresistance (MR) effect that is strongly correlated to a ferromagnetic and metallic state has been explained by a Zener's double exchange (DE) interaction with Jahn-Teller (JT) distortions in the MnO_6 octahedron.[6–9] Divalent dopants induce holes in the e_g band near the Fermi energy and e_g electrons become itinerant. This accounts for the electronic conduction and magnetic ordering. By the strong Hund's rule coupling, the spin of the e_g electron in Mn^{3+} is ferromagnetically coupled with the spin of the neighboring t_{2g} electron in Mn^{4+}, which enhances hopping of the e_g electron by the factor $\cos(\theta_{i,j}/2)$, where $\theta_{i,j}$ is the angle between the spins of their respective t_{2g} electrons.

In the low temperature ferromagnetic region, $T<T_C$, a dominant T^2 contribution in resistivity is generally observed and has been ascribed to electron-electron scattering or electron-magnon scattering.[5,10] An empirical T^n term, $n \sim 2.5$, is introduced to fit experimental results arising from a combination of electron-electron, electron-phonon, and electron-magnon scattering.[11] In addition, a $T^{4.5}$ contribution from two-magnon scattering has been derived from the quantum mechanical interpretation of the classical DE interactions.[12] Recently, a small polaron hopping model has been suggested as a prevalent mechanism for the low temperature electron conduction.[13]

As a crucial factor of the DE interaction, the ratio of Mn^{3+}/Mn^{4+} of multivalent Mn has become the main focus of manganese perovskite research. Many studies have been carried out by substituting rare earth atoms (A site) with divalent atoms (Ca, Sr, Ba, etc.) and also by introducing various transition metals onto the manganese, B site.[14–23]

The choice of interest to replace Mn ions is nonmagnetic Zr, having a 4+ valence state, no $3d$ electrons, and a larger ionic radius than the Mn ion. The unique electronic properties of nonmagnetic Zr together with its expected dilution of the magnetization should lead to the following: (1) an increase in the lattice volume from substitution of the larger Zr ion, (2) changes in the electron carrier density and the number of electron hopping sites, and (3) changes in the magnetic transition (T_C) arising from structural distortion of

a)Electronic mail: jinbo@umr.edu

 © 2007 American Institute of Physics

MnO_6 octahedra. In this paper, we report the effects of replacing Mn with Zr in the $La_{0.7}Sr_{0.3}MnO_3$ (LSMO) compound. The structural, magnetic, and electronic phase transitions and transport properties of $La_{0.7}Sr_{0.3}Mn_{1-x}Zr_xO_3$ with $0 \leqslant x \leqslant 0.20$ were investigated by neutron diffraction, magnetization, electrical resistivity, and magnetoresistance measurements.

II. EXPERIMENT

Zr-substituted $La_{0.7}Sr_{0.3}Mn_{1-x}Zr_xO_3$, with $0 \leqslant x \leqslant 0.20$, was synthesized by a conventional solid state reaction method. Highly purified La_2O_3, $SrCO_3$, MnO, and Zr metal were mixed in stoichiometric ratios, ground, and then pelletized at 3000 psi to 1 cm diameter. The pelletized samples were fired at 1500 °C in air for 12 h, and then reground and sintered at 1250 °C for 24 h in air. The sintered pellet removed from the oven at 900 °C was then cooled down to room temperature (RT). X-ray diffraction of the powders was carried out at room temperature using a SCINTAG diffractometer. Powder neutron diffraction experiments were performed at the University of Missouri-Columbia Research Reactor (MURR) using neutrons of wavelength $\lambda = 1.4875$ Å. The data for each sample were collected between $2\theta = 5.65°$ and 105.60° at 300 and at 10 K. Crystallographic structures of the samples were determined by Rietveld refinement of the neutron diffraction data using the FULLPROF program.[24] Magnetic measurements were performed using a Quantum Design superconducting quantum interference device (SQUID) magnetometer and resistivity data were obtained using a physical properties measurement system (PPMS) (Quantum Design) with a standard four-point probe method.

III. RESULTS AND DISCUSSION

In Fig. 1 x-ray diffraction patterns of $La_{0.7}Sr_{0.3}Mn_{1-x}Zr_xO_3$ at RT indicate that $x \leqslant 0.10$ samples are single phase and all peak positions are indexed to $La_{0.67}Sr_{0.33}MnO_{2.91}$ (Ref. 37), space-group $R\bar{3}c$. For $x \geqslant 0.15$, impurity phases appeared and were determined to be $SrZrO_3$ (Ref. 38) and $La_2Zr_2O_7$ (Ref. 39). Powder neutron diffraction (ND) was performed at RT and 10 K to investigate detailed structural distortion and magnetic structure in these compounds. Figure 2 shows the ND patterns of $La_{0.7}Sr_{0.3}Mn_{0.95}Zr_{0.05}O_3$ at RT and 10 K. All ND patterns were fitted well with the $R\bar{3}c$ rhombohedral space group with the atomic positions of La(Sr) at $6a(0,0,1/4)$, Mn(Zr) at $6b(0,0,0)$, and O at $18e(x,0,1/4)$. Even though all magnetic reflections may be indexed with the same nuclear cell, the $P1$ space group was used to fit the magnetic structure because of its flexibility. For the $x \geqslant 0.15$ samples, the $Pbnm$ and $Fd\bar{3}m$ space groups were used to refine the $SrZrO_3$ and $La_2Zr_2O_7$ phases. Magnetic contribution peaks are shown at $2\theta \approx 31.5°$ and 55.8°. Refined lattice parameters and magnetic moments for the $0 \leqslant x \leqslant 0.20$ samples are listed in Tables I and II.

Because the ionic radius of Zr^{4+} (0.72 Å) is larger than the ionic radii of Mn^{4+} (0.530 Å) and Mn^{3+} (0.645 Å), Zr^{4+} might be considered to substitute at (La^{3+}, Sr^{2+}) sites whose

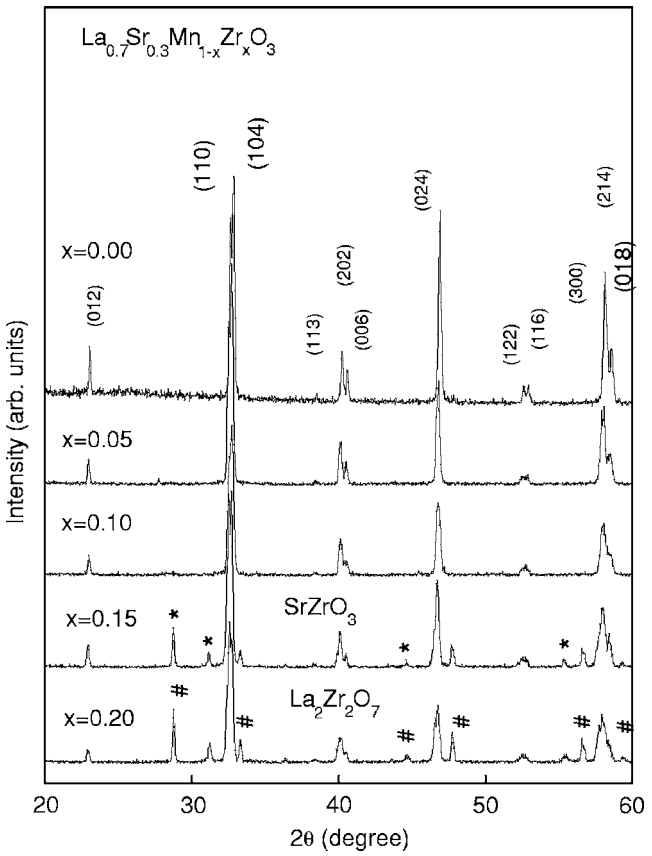

FIG. 1. X-ray diffraction patterns of $La_{0.7}Sr_{0.3}Mn_{1-x}Zr_xO_3$ ($x = 0.0, 0.05, 0.10, 0.15, 0.20$) at room temperature. Asterisks (*) indicate the diffraction peaks of $SrZrO_3$ and sharps (#) indicate the diffraction peaks of $La_2Zr_2O_7$.

ionic radii are 1.36 and 1.44 Å, respectively.[25] However, Rietveld refinement revealed that Zr^{4+} goes only to the Mn sites, which suggests that charge valence matching dominates ionic size matching with a resulting distortion of the MnO_6 octahedra in these systems. This result is different from that reported by Roy and Ali.[26] Similar to previous studies of Zr-substituted $La_{1-x}Ca_xMnO_3$,[27,28] the Zr-solubility limit occurs around $x = 0.10$ and beyond that, excess Zr forms $SrZrO_3$ and La_2Zr_2O7 phases.

For a perovskite structure, the solubility limit may be predicted by calculating the valence state of the dopants and the critical tolerance factor τ, which is defined as $(r_{(La,Sr)} + r_O)/[(r_{(Mn,Zr)} + r_O)\sqrt{2}]$, where r is the average ionic radius.[3,29] The tolerance factors of $La_{0.7}Sr_{0.0}Mn_{1-x}Zr_xO_3$ decrease linearly from 0.978 to 0.970 for LSMO and $x = 0.10$, respectively. Considering the increments of the Mn–O bond length and $r_{(Mn,Zr)}$ with increasing Zr content (Fig. 3), Zr^{4+} may replace Mn^{4+}, not Mn^{3+}, which gives about a three times larger increment than the measured value. Therefore Zr^{4+} substitution for Mn^{4+} produces ZrO_6 octahedra, which give rise to larger strains in the local MnO_6 chains and induce a local distortion which prohibits further Zr dissolution. However, considering the stability range of LSMO $0.89 < \tau < 1.02$, the Zr-solubility limit into LSMO at $x \sim 0.10$ is relatively low. Two other explanations may be possible for the low Zr-solubility limit: oxygen deficiency and interdiffusion between LSMO and Zr compounds. At the $x = 0.10$ sample,

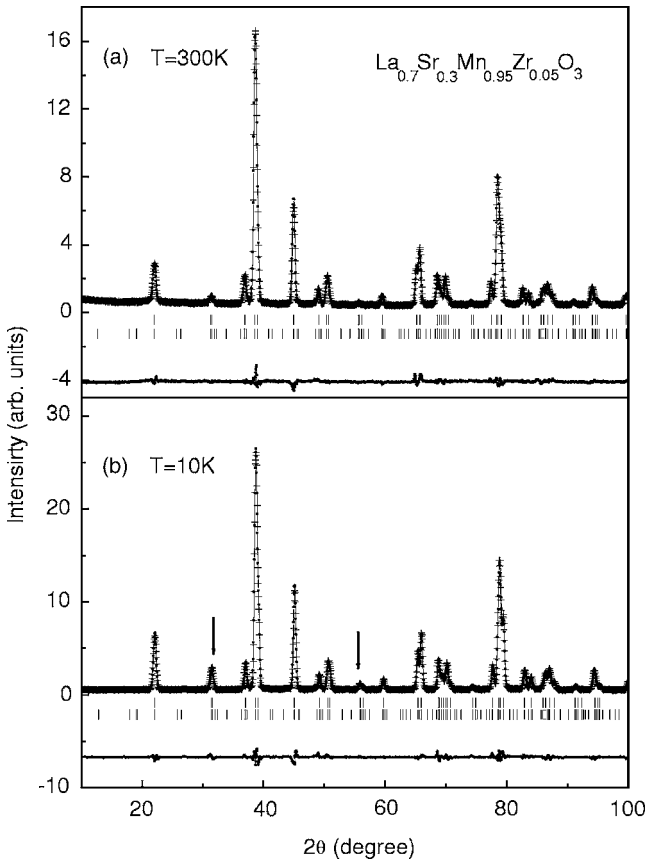

FIG. 2. Neutron diffraction patterns of $La_{0.7}Sr_{0.3}Mn_{0.95}Zr_{0.05}O_3$ at room temperature and at 10 K. Arrows indicate some of the major magnetic contribution peaks.

about 4.8% oxygen deficiency was observed from ND data. If we assume that there are no vacancies at the (La, Sr) *A* sites, the oxygen deficiency drives the reduction of Mn^{4+} to Mn^{3+} in order to maintain a charge balance. Thus as the larger Mn^{3+} replaces Mn^{4+}, Zr^{4+} substitution at the *B* site is reduced. As the ionic radius of O^{2-} (1.4 Å) is larger than Mn^{3+}, oxygen deficiency will also slightly reduce the average (Mn, Zr)–O bond length. The above reasoning is probably not the only explanation if one considers the work of Lau and Singhal,[30] wherein they observed interdiffusion occurring across the interface between $(La,Sr)MnO_3$ and yttrium-stabilized ZrO_2 (YSZ). In particular, the dissolution of Mn^{3+} into ZrO_2 produces thermodynamically stable $La_2Zr_2O_7$ with other Mn-substituted Zr oxides and accordingly lowers the Zr-solubility limit. Magnetization measurements of $x=0.20$ in Fig. 4 confirm the existence of a Zr-solubility limit at $x\sim0.10$ and interdiffusion between LSMO and zirconates with its two magnetic transition temperatures.

The lattice parameters *a* and *c* and the lattice volume for $x\leqslant0.05$ increase with increasing Zr content and then remain nearly constant at $x=0.10$. There is essentially no oxygen deficiency for $x\leqslant0.05$, but as mentioned above, 4.8% of oxygen deficiency is calculated at $x=0.10$. The changes in average bond length and bond angle resulting from the ionic size mismatch on the Mn *B* site, the oxygen deficiency, and the exchange interactions between Mn–Mn determine the nature of the electronic phase transition and the magnitude of the magnetic ordering temperature T_C. Since the effective *d*-electron transfer interaction between the neighboring Mn sites is governed by the exchange interaction via the O 2*p* state, the electronic bandwidth *W* has been frequently used to explain the magnetic and transport properties of ABO_3-type perovskites. Using the tight binding approximation, the bandwidth *W* for a charge-transfer insulator is $w \propto \cos\omega/(d_{Mn-O})^{3.5}$, where $\omega=\frac{1}{2}(\pi-\langle Mn-O-Mn\rangle)$, d_{Mn-O} is the Mn–O bond length, and $\langle Mn-O-Mn\rangle$ is the average bond angle.[31,32] Figure 3 shows the Mn–O bond length, Mn–O–Mn bond angle, and calculated bandwidths *W* as a function of *x*. Up to $x=0.10$, the average bond angle decreases continuously with increasing Zr content while the average (Mn,Zr)–O bond length increases. The one-electron bandwidth *W* decreases with increasing Zr content at RT and 10 K. The decrease in bandwidth indicates a reduction in the overlap between the O 2*p* and Mn 3*d* orbitals, which weakens the ferromagnetic exchange coupling of Mn^{3+}–Mn^{4+}. This in turn decreases the magnetic ordering temperature T_C.[16]

TABLE I. Refined parameters for $La_{0.7}Sr_{0.3}Mn_{1-x}Zr_xO_3$ compound ($x=0.0$, 0.03, 0.05, 0.10, 0.15, 0.20) with $R\bar{3}c$ space group at room temperature ($T=300$ K). For $x\leqslant0.15$ samples, *Pbnm* and $Fd\bar{3}m$ space groups are used to refine the phases of $SrZrO_3$ and $La_2Zr_2O_7$ and they are not listed in this table. Numbers in parentheses are statistical errors. *a* and *c* are the lattice parameters. *V* is the unit cell volume. *m* is magnetic moment. O(occ) is site occupation number of oxygen. χ^2 is $[R_{wp}/R_{exp}]^2$, where R_{wp} is the residual error of the weighted profile. Oxygen occupation number of $x=0.10$ is fixed with the refined value at $T=10$ K measurement, and oxygen occupation number of $x\leqslant0.15$ is fixed with the original stoichiometric value.

x	0.00	0.03	0.05	0.10	0.15	0.20
A (Å)	5.5038(2)	5.5119(2)	5.5231(2)	5.5246(3)	5.5240(3)	5.5304(4)
c (Å)	13.3553(5)	13.3643(5)	13.3883(6)	13.3902(8)	13.3928(8)	13.4128(15)
V (Å^3)	350.364(18)	351.618(2)	352.639(2)	353.928(3)	353.268(5)	355.127(6)
m (μ_B)	2.514(28)	2.207(46)	1.956(33)	1.307(50)	1.320(79)	1.393(112)
χ^2 (%)	2.81	3.07	3.46	4.04	4.48	5.14
O, 18*e*,*x*	0.5422(2)	0.5437(2)	0.5449(2)	0.5458(2)	0.5454(2)	0.5475(2)
O, 18*e* (occ.)	0.498(3)	0.493(3)	0.492(2)	0.476(3)*	0.500	0.500
B (Å^2), La(Sr), 6*a*	0.882(33)	0.935(40)	0.893(34)	1.069(49)	0.895(51)	0.805(68)
B (Å^2), Mn(Zr), 6*b*	0.423(54)	0.392(69)	0.197(61)	0.462(86)	0.985(142)	0.803(197)
B (Å^2), O, 18*e*	1.221(25)	1.342(30)	1.384(25)	1.502(34)	1.394(36)	1.340(481)

TABLE II. Refined parameters for $La_{0.7}Sr_{0.3}Mn_{1-x}Zr_xO_3$ compound (x=0.0, 0.03, 0.05, 0.10, 0.15, 0.20) with $R\bar{3}c$ space group at T=10 K. For $x \geqslant 0.15$ samples, *Pbnm* and $Fd\bar{3}m$ space groups are used to refine the phases of $SrZrO_3$ and $La_2Zr_2O_7$ and they are not listed in this table. Numbers in parentheses are statistical errors. a and c are the lattice parameters. V is the unit cell volume. m is magnetic moment. O(occ) is site occupation number of oxygen. χ^2 is $[R_{wp}/R_{exp}]^2$, where R_{wp} is the residual error of the weighted profile. Oxygen occupation number of $x \geqslant 0.15$ is fixed with the original stoichiometric value.

x	0.00	0.03	0.05	0.10	0.15	0.20
a (Å)	5.4811(1)	5.5007(2)	5.5070(1)	5.5088(2)	5.5018(2)	5.5080(4)
c (Å)	13.2756(3)	13.3170(5)	13.3314(4)	13.3355(6)	13.3177(7)	13.3491(15)
V (Å^3)	345.397(1)	348.960(2)	350.132(2)	350.475(2)	349.169(3)	350.732(5)
m (μ_B)	3.543(25)	3.535(32)	3.447(23)	3.297(27)	3.742(40)	3.274(50)
χ^2 (%)	3.23	2.94	3.98	3.83	4.54	5.16
O, 18e,x	0.5431(1)	0.5445(1)	0.5448(1)	0.5461(2)	0.5437(2)	0.5452(3)
O, 18e (occ)	0.503(3)	0.497(3)	0.500(2)	0.476(3)	0.500	0.500
B (Å^2), La(Sr), 6a	0.167(23)	0.255(36)	0.343(25)	0.236(35)	0.680(54)	0.485(83)
B (Å^2), Mn(Zr), 6b	0.127(45)	0.104(65)	0.034(48)	0.393(101)	0.479(146)	0.527(224)
B (Å^2), O, 18e	0.328(21)	0.519(28)	0.703(20)	0.575(26)	0.949(36)	0.899(54)

Figure 4 shows magnetization as a function of temperature (M-T) under field-cooled (FC) and zero-field-cooled (ZFC) conditions in a magnetic field of 50 Oe. Magnetic transition temperatures are obtained with T_C=367, 350, 343, and 315 K for x=0.00, 0.03, 0.05, and 0.10, respectively. A sharp ferromagnetic to paramagnetic transition is observed for $x \leqslant 0.03$, and the transition curves of the $x \geqslant 0.05$ samples become broad. A λ-shaped magnetization curve in ZFC emerges at x=0.10, which may suggest an order-disorder transition of ferromagnetic clusters near T_C. Two magnetic transition temperatures are observed for $x \geqslant 0.15$ samples: a higher $T_{C1} \sim 317$ K for Zr-substituted LSMO and a lower $T_{C2} \sim 235$ K for Mn-interdiffused zirconates. The higher T_{C1} is almost the same as the T_C of the 10% Zr-substituted LSMO, which may be explained as the formation of $La_{0.7}Sr_{0.3}Mn_{0.9\pm\delta}Zr_{0.1\mp\delta}O_3$ with other Zr-containing oxides.

The values of the magnetic moments from the saturation magnetization measurements at T=10 K, 3.60, 3.44, and 3.36 μ_B, agree well with the magnetic moments from the ND data at T=10 K, Table II. Since ND measures only localized moments, the values from bulk magnetic saturation magne-

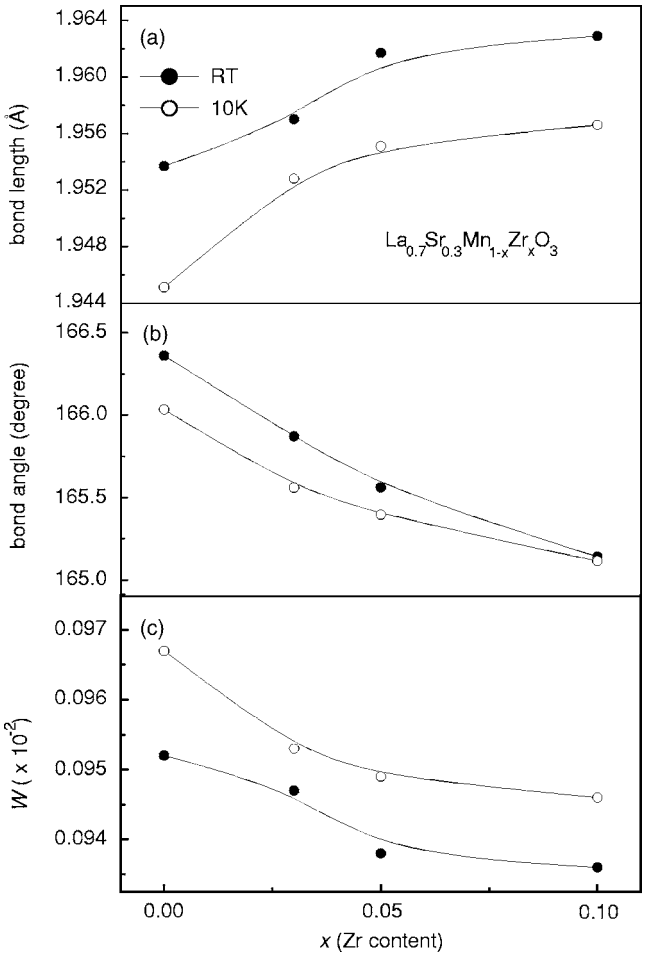

FIG. 3. (a) Average (Mn,Zr)–O bond lengths, (b) (Mn,Zr)–O–(Mn,Zr) bond angles, and (c) electronic bandwidth parameter, $\cos(\omega)/d_{Mn-O}^{3.5}$ of $La_{0.7}Sr_{0.3}Mn_{1-x}Zr_xO_3$ (x=0.0, 0.03, 0.05, 0.10) at room temperature and at 10 K.

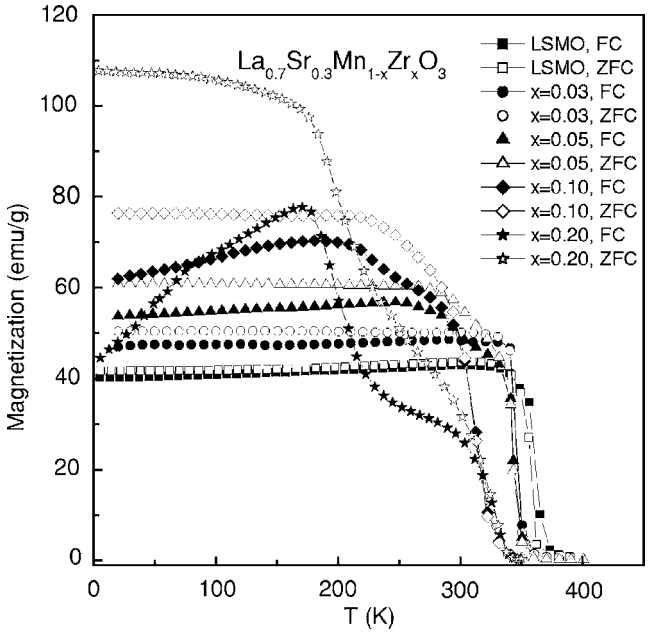

FIG. 4. The magnetization vs temperature curves of $La_{0.7}Sr_{0.3}Mn_{1-x}Zr_xO_3$ (x=0.0, 0.03, 0.05, 0.10, 0.20) measured under field cooling (FC) and zero field cooling (ZFC) conditions in a magnetic field of 50 Oe.

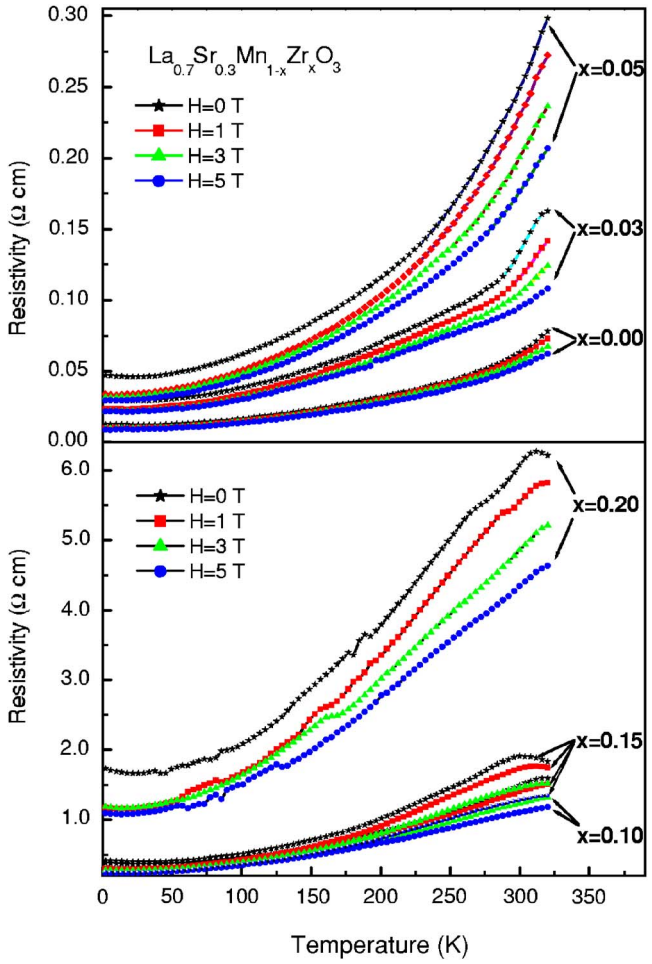

FIG. 5. (Color online) Temperature dependence of resistivity of $La_{0.7}Sr_{0.3}Mn_{1-x}Zr_xO_3$ (x=0.0, 0.03, 0.05, 0.10, 0.15, 0.20) under magnetic fields of H=0, 1, 3, 5 T.

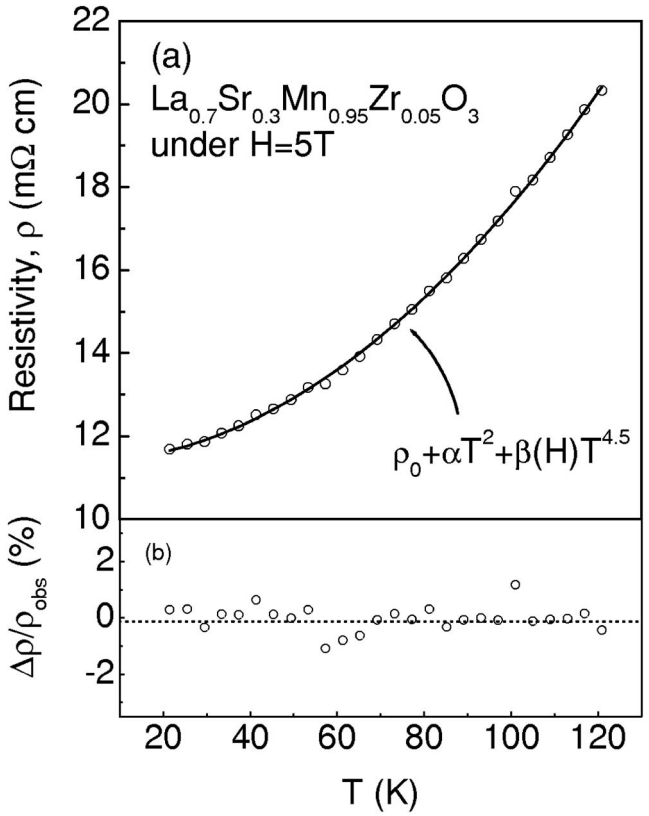

FIG. 6. (a) The fitting curve of the resistivity of $La_{0.7}Sr_{0.3}Mn_{0.95}Zr_{0.05}O_3$ under H=5 T in the low temperature region. (b) The relative deviation $[\Delta\rho/\rho_{obs}(\%)]$ between observed data and fitted curve in (a).

tization measurements are slightly larger than those of the ND measurements. When we consider the magnetic moments of Mn from its valence states with a spin only moment, taking into account the dilution effect of nonmagnetic Zr^{4+}, we obtain larger values of 3.61, 3.55, and 3.40 μ_B per Mn atom, for x=0.03, 0.05, and 0.10, respectively, in good agreement with the ND results.

Figure 5 shows resistivity as a function of temperature under different applied fields for $La_{0.7}Sr_{0.3}Mn_{1-x}Zr_xO_3$ compounds with x=0.0, 0.03, 0.05, 0.10, 0.15, and 0.20. All samples show a residual resistivity (ρ_0) below $T\sim$40 K, and ρ_0 increases with increasing Zr content. The temperature independent ρ_0 may be ascribed to scattering processes that arise from randomly distributed defects, oxygen vacancies, and the grain boundaries. Because of contributions from the inhomogeneous character of grain and domain boundaries, the ρ_0 of polycrystalline LSMO is larger than that observed for films and single crystal samples.[33] The sudden increase of ρ_0 between x=0.05 and x=0.10 may be due to the insulator-rich grain boundaries induced by the oxygen deficiency.

In the previous studies of the low temperature ($T<T_C$) resistivity in the various kinds of rare earth manganites, several different equations have been used to characterized the resistivity behavior. The low temperature resistivity of LSMO has been well described by the T^2 term, which was interpreted as being due to an electron-electron scattering,[5] while the $T^{2.5}$ dependency has been shown in $La_{1-x}Ca_xMnO_3$ (LCMO) compounds.[11] As our samples are in the ferromagnetic metal phase in the low temperature region, the magnon-relevant scattering contribution to the resistivity can be predicted. Therefore, additional $T^{4.5}$ dependency needs to be considered due to the 100% polarized two-magnon scattering process derived from the quantum mechanical interpretation of the double exchange mechanism.[12] After fitting several models within a limited temperature range, 20 K$\leqslant T\leqslant$120 K, we obtained better agreement with the following equation:

$$\rho = \rho_0 + \alpha T^2 + \beta(H)T^{4.5}, \tag{1}$$

where ρ_0 is residual resistivity, α is a field independent term of the electron-electron scattering process, and $\beta(H)$ is a field dependent term of the two-magnon scattering process. Taking into consideration the electron-electron and two-magnon scattering processes, the results of the fitting with Eq. (1) in the low temperature ferromagnetic region for $La_{0.7}Sr_{0.3}MnO_3$ under H=5 T are shown in Fig. 6(a). The relative difference $\Delta\rho/\rho$ between the data and fitted curve is plotted in Fig. 6(b). The residuals of Eq. (1) appear as random errors without any systematic deviation, which suggests that the model is reliable. Table III lists the fitting parameters for Eq. (1) in the temperature range 20 $K\leqslant T\leqslant$120 K, under H=0 and 5 T.

TABLE III. Fitting parameters of model I for the temperature dependence of resistivity in low temperature region (20–120 K) using $\rho=\rho_0+\alpha T^2+\beta(H)T^{4.5}$ for $La_{0.7}Sr_{0.3}Mn_{1-x}Zr_xO_3$, $x=0.00$, 0.03, 0.05, and 0.10, under $H=0$ and 5 T. Adjusted R^2 was calculated with $1-[(n-1)\Sigma_{i=1}^{n}w_i(\hat{y}_i-\bar{y})^2]/[(n-m-1)\Sigma_{i=1}^{n}w_i(y_i-\bar{y})^2]$, where n is the number of data points, m is the number of fitted points, y_i is the observed value, $\hat{y}_i$ is the fitted value, and ω is the weight.

x	$\rho_0(H=0)$ (Ω cm)	α (Ω cm K^{-2})	$\beta(H=0)$ (Ω cm K$^{-4.5}$)	Adjusted R^2
0.00	0.0026	0.938×10^{-7}	1.229×10^{-13}	0.9958
0.03	0.0111	3.400×10^{-7}	3.497×10^{-13}	0.9979
0.05	0.0175	6.143×10^{-7}	4.184×10^{-13}	0.9986
0.10	0.1048	2.290×10^{-6}	6.118×10^{-12}	0.9955
x	$\rho_0(H=5$ T) (Ω cm)	α (Ω cm K^{-2})	$\beta(H=5$ T) (Ω cm K$^{-4.5}$)	Adjusted R^2
0.00	0.0020	1.042×10^{-7}	0.167×10^{-13}	0.9967
0.03	0.0082	3.346×10^{-7}	1.729×10^{-13}	0.9983
0.05	0.0114	6.188×10^{-7}	2.085×10^{-13}	0.9993
0.10	0.0702	3.234×10^{-6}	3.278×10^{-13}	0.9996

At low temperatures, a dominant T^2 dependence of resistivity is manifested because the charge carriers are spin polarized and the first order spin-wave interaction decreases exponentially with decreasing temperature. We did not observed any reduction in the contribution of the T^2 term to the low temperature resistivity, which is interpreted as an indication of a single-magnon scattering process.[34] In this temperature region, more than 95% of resistivity is described by the T^2 term for all samples. Figure 7 shows the reduction in the contribution of resistivity with T^2 with increasing temperature. The contribution of resistivity from the $T^{4.5}$ term increases with increasing temperature. For the $x=0.03$ sample under $H=0$ and 5 T, the contribution from the $T^{4.5}$ term rapidly increases from 4.15% to 27.85% of the total resistivity at $T=50$ K and from 1.64% to 12.92% at 120 K.

For the low temperature region, all the magnetic moments in the ferromagnetic metal are completely spin polarized. When the temperature increases, the localized moments begin to be thermally agitated and both phonons and magnons are excited and interact with the conducting electrons. Because the magnon is disturbed more readily than the lattice phonon with increasing temperature, the resistivity due to the magnon becomes larger up to T_C. The suppression of resistivity by the applied magnetic field occurs in all samples. According to the DE mechanism, the mobility of the charge carrier e_g electron improves if the neighboring t_{2g} spins are ferromagnetically polarized. The applied field aligns the electron spins which should reduce the scattering of the itinerant electrons, and thus the resistivity from the electron-magnon and magnon-magnon scattering is reduced. As expected, when the magnetic field is applied, the $T^{4.5}$ term decreases rapidly. For the $x=0.03$ sample at $T=100$ K, the contribution to the total resistivity drops from 19.66% to 8.60% and at $T=120$ K, and the contribution to the total resistivity drops from 27.85% to 12.92%, both under $H=5$ T, Fig. 7.

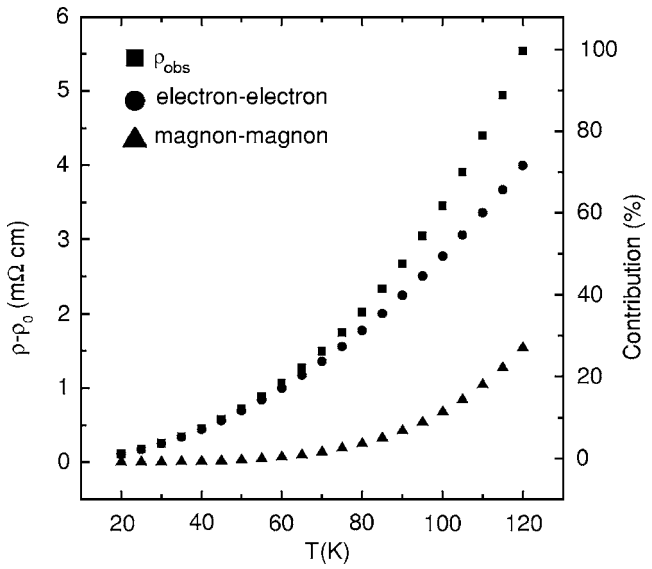

FIG. 7. The respective contributions to the total resistivity from the electron-electron (T^2 term) and two-magnon ($T^{4.5}$ term) scattering processes in $La_{0.7}Sr_{0.3}Mn_{0.97}Zr_{0.03}O_3$ in a magnetic field of $H=0$ T.

According to the Fermi liquid model, the electron-electron scattering process gives a T^2 dependency of the resistivity but not necessarily the field dependency.[35] A previous study has reported the α term to be field independent within 10%.[33] Fits to our data in various fields confirm the field independence of α for $x\leqslant0.05$ within ±2%. For $x=0.10$, α increases by about 40% under $H=5$ T, which may be ascribed to grain boundary effects.

Several other models were also tested and compared with the model of Eq. (1). A simple $\rho=\rho_0+\alpha(H)T^2$ model, which considered electron-magnon interactions with the field dependent coefficient $\alpha(H)$, fitted well in the limited low temperature region but failed above $T=100$ K. An experimentally based empirical model $\rho=\rho_0+\alpha(H)T^n$ with various powers of T also fitted with $2.4\leqslant n\leqslant2.9$, but n varied irregularly with the Zr content. In addition, other models displayed that the residuals have systematic patterns as a sign of unreliable fitting. The upturn of the resistivity at $T\sim20$ K occurs for all samples, which may indicate the localization of charge carriers and grain boundary effects as seen in $La_{1-x}Sr_xMnO_3$ near the metal to insulator transition.[36]

Figure 8 shows the temperature dependence of the magnetoresistance (MR) of $La_{0.7}Sr_{0.3}Mn_{1-x}Zr_xO_3$ with $x=0.03$ and 0.10 under applied fields of $H=1$, 3, and 5 T using

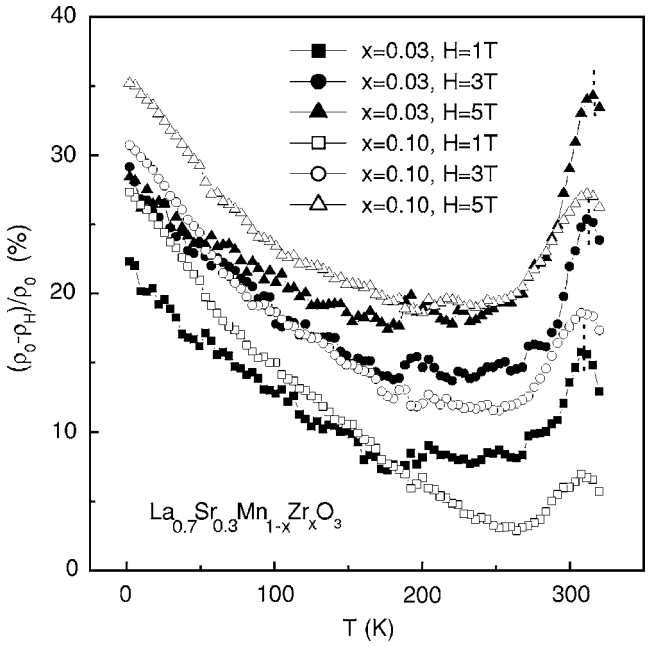

FIG. 8. Temperature dependence of magnetoresistance of $La_{0.7}Sr_{0.3}Mn_{1-x}Zr_xO_3$ ($x=0.03,0.10$) under magnetic fields of $H=1,3,5$ T.

$MR=(\rho_0-\rho H)/\rho_0\times 100$. The maximum MR peaks, MR_{max}, become weaker and broader with increasing Zr content for the $x\leqslant 0.10$ samples. The MR_{max} shifts to a higher temperature region upon application of an external magnetic field. A MR_{max} of 35% was obtained at $T=303$ K with the $x=0.03$ sample under $H=5$ T.

In conclusion, it is both interesting and informative to compare the results of our studies with other substituted LSMO made with replacement of the Mn B site by $3d$ transition metals (TMs).[14–23] The TM-substituted LSMOs all have the $R\bar{3}c$ space group and exhibited a decrease in T_C and a metal to insulator transition (MIT) occurs with increasing substitution. However, the degree of reduction in T_C and saturation magnetization is proportional mainly to the ionic size mismatch in the case of Zr^{4+}. These effects are proportional to both the magnetic moments and ionic size mismatch of the TM ions. In this regard, the highest T_C's are obtained for Cr- and Co-substituted LSMOs.[18,20] These are attributed mainly to the large magnetic moments of Cr and Co ions and to the formation of additional DE interactions Cr/Mn and Co/Mn. In the case of Cr, Kallel *et al.*[18] propose that a ferromagnetic DE interaction between Mn and Cr is formed through the following dynamic oxidation-reduction process: $Mn^{3+}+Cr^{3+}\leftrightarrow Mn^{4+}+Cr^{2+}$. With increasing Cr content, the $Mn^{3+}-O-Mn^{4+}$ chains are replaced by $Mn^{3+}-O-Cr^{3+}$. However, the Cr chains are not equivalent to the Mn chains because of the large deviation from 180° of the bond angle of the $Mn^{3+}-O-Cr^{3+}$ and $Mn^{4+}-O-Cr^{2+}$ chains. Thus the randomly replaced Cr chains weaken the ferromagnetic ordering and charge transfer. An interesting paper by Sotirova-Haralambeva *et al.*[17] present a study of the replacement of Mn in LSMO with nonmagnetic Zn ions. Similarly to our Zr^{4+} substituted LSMO, their magnetization decreased (but considerably more than for Zr^{4+} substitution) with increasing Zn^{2+} concentration, and above $x=0.2$ ferromagnetic ordering is lost and the material becomes paramagnetic. Within the same concentration range, we do not observe such a transition. Their transport properties which show a decrease in the MIT with increasing Zn concentration and the increase in resistivity with increasing Zn concentration $0<x<0.1$ are consistent with our results for Zr. They attribute their results mainly to the fact that the nonmagnetic Zn ion cannot participate in the double exchange: $Mn^{3+}-O-Zn^{2+}$. This is in agreement with our proposed mechanism except that we also consider the contribution of the ionic size mismatch in producing distortion of the oxygen octahedral with subsequent deviation of the DE chains from 180°.

IV. SUMMARY

The changes in the magnetic and electronic transport properties of Zr-substituted $La_{1-x}Sr_xMnO_3$ were systematically investigated. Up to 10% Zr-substituted $La_{1-x}Sr_xMnO_3$, the compounds have a rhombohedral structure with the $R\bar{3}c$ space group. Beyond 10%, Zr substitution results in the formation of $SrZrO_3$ and $La_2Zr_2O_7$ impurity phases. The decrease of the bandwidth W decreases the overlap between the O $2p$ and Mn $3d$ orbitals, which decreases the exchange coupling of Mn–Mn and the magnetic ordering temperature T_C as well. The resistivity for the $20\ \text{K}\leqslant T\leqslant 120$ K region exhibits metallic behavior and fits well with an electron-electron and two-magnon scattering model. The electron-electron scattering process is dominant in the low temperature region and a two-magnon scattering process emerges with increasing temperature.

ACKNOWLEDGMENTS

The authors thank Aranwela Hemantha for invaluable help in the magnetoresistance measurements. The support by DOE under DOE Contract No. DE-FC26-99FT400054 is acknowledged.

[1] C. W. Searle and S. T. Wang, Can. J. Phys. **47**, 2703 (1969).
[2] S. Jin, T. H. Tiefel, M. McCoemack, R. A. Fastnacht, R. Ramesh, and L. H. Chen, Science **264**, 413 (1994).
[3] J. B. Goodenough, *Magnetism and the Chemical Bond* (Interscience, New York, 1963).
[4] R. von Helmolt, J. Wecker, B. Holzapfel, L. Schultz, and K. Samwer, Phys. Rev. Lett. **71**, 2331 (1993).
[5] A. Unishibara, Y. Moritomo, T. Arima, A. Asamitsu, G. Kido, and Y. Tokura, Phys. Rev. B **51**, 14103 (1995).
[6] A. Zener, Phys. Rev. **82**, 403 (1951).
[7] P. W. Anderson and H. Hasegawa, Phys. Rev. **100**, 675 (1955).
[8] P. G. de Gennes, Phys. Rev. **118**, 141 (1960).
[9] A. J. Millis, P. B. Littlewood, and B. I. Shraiman, Phys. Rev. Lett. **74**, 5144 (1995).
[10] L. Mannari, Prog. Theor. Phys. **22**, 335 (1959).
[11] P. Schiffer, A. P. Raminez, W. Bao, and S. W. Cheong, Phys. Rev. Lett. **75**, 3336 (1995).
[12] K. Kubo and N. Ohata, J. Phys. Soc. Jpn. **33**, 21 (1972).
[13] A. S. Alexandrov and A. M. Bratkovsky, Phys. Rev. Lett. **82**, 141 (1999).
[14] C. Martin, A. Maignan, and B. Raveau, J. Mater. Chem. **6**, 1245 (1996).
[15] M. S. Kim *et al.*, Phys. Rev. B **71**, 014433 (2005).
[16] M. S. Kim *et al.*, J. Appl. Phys. **97**, 10H714 (2005).
[17] E. V. Sotirova-Haralambeva, X. L. Wang, K. H. Liu, T. Silver, K. Konstantinov, and J. Horvat, Sci. Technol. Adv. Mater. **4**, 149 (2003).
[18] N. Kallel, K. Froehlich, M. Oumezzine, M. Ghedira, H. Vicent, and S. Pignard, Phys. Status Solidi C **1**, 1649 (2004).
[19] O. Z. Yanchevskli, O. I. Vyunov, A. G. Belous, and A. I. Tovstolytkin, Low Temp. Phys. **32**, 134 (2006).

[20]J. B. Shi, F. C. Wu, and C. T. Lin, Appl. Phys. A: Mater. Sci. Process. **68**, 577 (1999).
[21]M. M. Xavier, F. A. O. Cabral, J. H. de Araujo, C. Chesman, T. Dumelow, and J. M. Sasaki, J. Magn. Magn. Mater. **223**, 826 (2001).
[22]D. N. H. Nam, L. V. Bau, N. V. Khiem, N. V. Dai, L. V. Hong, N. X. Phuc, R. S. Newrock, and P. Nordblad, Phys. Rev. B **73**, 184430 (2006).
[23]Q. Zhou, M. Dai, R. Wang, C. Liu, G. Zhang, D. Ai, and J. Feng, Physica B **371**, 120 (2006).
[24]J. Rodriguez-Carvajal, program FULLPROF, Version 3.5d.
[25]R. D. Shannon, Acta Crystallogr., Sect. A: Cryst. Phys., Diffr., Theor. Gen. Crystallogr. **32**, 751 (1976).
[26]S. Roy and N. Ali, J. Appl. Phys. **89**, 7425 (2001).
[27]H. Yokokawa, Annu. Rev. Mater. Sci. **33**, 581 (2003).
[28]D. Das, A. Saha, S. E. Russek, R. Raj, and D. Bahadur, J. Appl. Phys. **93**, 8301 (2003).
[29]M. Mirzadeh and M. Akhavan, Eur. Phys. J. B **43**, 305 (2005).
[30]S. K. Lau and S. C. Singhal, Corrosion (Houston) **85**, 345 (1985).
[31]H. Y. Hwang, S.-W. Cheong, P. G. Radaelli, M. Marezio, and B. Batlogg, Phys. Rev. Lett. **75**, 914 (1995).
[32]P. G. Radaelli, G. Iannone, M. Marezio, H. Y. Hwang, S.-W. Cheong, J. D. Jorgensen, and D. N. Argyriou, Phys. Rev. B **56**, 8265 (1997).
[33]G. J. Snyder, R. Hiskes, S. DiCarolis, M. R. Beasley, and T. H. Geballe, Phys. Rev. B **53**, 14434 (1996).
[34]M. Jaime, P. Lin, M. B. Salomon, and P. D. Han, Phys. Rev. B **58**, R5901 (1998).
[35]A. H. Thompson, Phys. Rev. Lett. **35**, 1786 (1975).
[36]T. Okuda, A. Asamitsu, Y. Tomioka, Y. Taguchi, and Y. Tokura, Phys. Rev. Lett. **81**, 3203 (1998).
[37]JCPDS-International Center for Diffraction Data, Card No. 50-0308 (Ref.: V. Zubkov, Inst. of Solid State Chemistry, Ekaterinburg, Russia, ICDD Grant in-Aid (1998).)
[38]JCPDS-International Center for Diffraction Data, Card No. 76-0167 (Ref.: Calculated from ICSD using POWD-12 ++, (1997); W. H. Zachariasen, Skr. Nor. Vidensk.-Akad., Kl. 1: Mat.-Naturvidensk. Kl., 1928, 1 (1928).)
[39]JCPDS-International Center for Diffraction Data, Card No. 71-2363 (Ref.: H. J. Deiseroth and H. Muller-Buschbaum, Z. Anorg. Allg. Chem. **375**, 152 (1970).)